Quantum Dot Single Photon Sources Studied with Superconducting Single Photon Detectors

Martin J. Stevens, Robert H. Hadfield, Robert E. Schwall, *Senior Member, IEEE*, Sae Woo Nam, *Member, IEEE*, and Richard P. Mirin, *Senior Member, IEEE*

(Invited Paper)

***Abstract*—We report the observation of photon antibunching from a single, self-assembled InGaAs quantum dot (QD) at temperatures up to 135 K. The second-order intensity correlation, $g^{(2)}(0)$, is less than 0.260 ± 0.024 for temperatures up to 100 K. At 120 K, $g^{(2)}(0)$ increases to about 0.471, which is slightly less than the second-order intensity correlation expected from two independent single emitters. In addition, we characterize the performance of a superconducting single photon detector (SSPD) based on a nanopatterned niobium nitride wire that exhibits 68 ± 3-ps timing jitter and less than 100-Hz dark count rate with a detection efficiency (DE) of up to 2% at 902 nm. This detector is used to measure spontaneous emission lifetimes of semiconductor quantum wells (QWs) emitting light at wavelengths of 935 and 1245 nm. The sensitivity to wavelengths longer than 1 μm and the Gaussian temporal response of this superconducting detector present clear advantages over the conventional detector technologies. We also use this detector to characterize the emission from a single InGaAs QD embedded in a micropillar cavity, measuring a spontaneous emission lifetime of 370 ps and a $g^{(2)}(0)$ of 0.24 ± 0.03.**

***Index Terms*—Infrared detectors, light sources, quantum dots (QDs), superconducting device measurements, superconducting radiation detectors.**

I. Introduction

SINGLE photonics is an area of increasing interest in the scientific community because of the recent emergence of a variety of fundamental measurements and advanced applications. One example is quantum key distribution (QKD), which provides a secure method of communicating between two parties [1]. Another is time-correlated single photon counting (TCSPC), which is a widely used method for measuring the spontaneous emission lifetime of semiconductors and molecules, as well as for biomedical imaging [2]; however, this technique typically has been limited to materials and specimens that emit at wavelengths shorter than about 1000 nm. In both of these applications, progress has been limited either by the performance of single photon sources or by the available single photon detectors. Numerous other applications are enabled by improvements in the generation and detection of single photons. Applications in the realm of fundamental science include loophole-free demonstration of Bell's inequality [3], generation of engineered quantum states of light [4]–[7], single photon metrology, and low light level spectroscopy. Industrial applications include precision light detection and ranging (LIDAR) [8] and the identification of silicon transistor switching defects via picosecond imaging circuit analysis (PICA) [9].

The most common and straightforward way to generate single photons is to use a heavily attenuated pulsed laser. The laser produces some average power with a mean photon number per pulse of N. It is relatively straightforward to use neutral density filters to attenuate the power until $N \leq 1$. The drawback to this method is that the photon number distribution obeys Poisson statistics, which means that the probability of getting zero or two photons is also quite high. In QKD demonstrations, N is typically set at 0.1, which means that most of the pulses contain no photons at all. Thus, an attenuated laser is inherently a low-efficiency single photon source. For these reasons, research has focused on the use of the single quantum emitters as potential on-demand single photon sources. Several different approaches have demonstrated single photon emission [10], including single atoms and ions [11]–[15], epitaxial InGaAs/GaAs quantum dots (QDs) [16], [17], epitaxial [18] and colloidal [19] CdSe QDs, GaAs interface fluctuation QDs [20], single molecules [21], and nitrogen vacancy (NV) color centers in artificial diamond [22] The ideal on-demand single photon source would be compact and stable, operate at or near room temperature, and have a short spontaneous emission lifetime to allow high speed operation. Most importantly, it would emit exactly one photon for each pump pulse.

Colloidal CdSe QDs and NV centers have demonstrated room-temperature single photon emission, but both exhibit degraded efficiencies due to blinking [19], [22] Single molecules can also emit at room temperature, but can exhibit photobleaching, at which point the molecules no longer emit any photons. Each of these sources is difficult to integrate with a microcavity, which is essential for decreasing the spontaneous emission lifetime and can enhance collection efficiency of the emitted photons. More importantly, coupling a source to a cavity can lead to a transform-limited emission, which is needed to ensure that successively emitted photons are indistinguishable from one another. The ability to generate indistinguishable photons is essential for more advanced applications such as linear optical quantum computing [23] and the development of engineered quantum states of light [4]–[7]. Atoms and ions, on the other hand, are easily integrated with cavities and can produce single

Manuscipt received March 15, 2006; revised September 15, 2006. This work was supported in part by the U.S. Department of Commerce and in part by the Defense Advanced Research Projects Agency (DARPA) Quantum Information Science and Technology (QuIST).

The authors are with the National Institute of Standards and Technology, Boulder, CO 80305 USA (e-mail: marty@boulder.nist.gov).

Digital Object Identifier 10.1109/JSTQE.2006.885088

photons [11]–[13], identical single photons [14], and entangled photon pairs [15]. The main disadvantages of atoms and ions are the relatively complex trapping apparatus required and the relatively long spontaneous emission lifetimes. In contrast, epitaxial InGaAs/GaAs QDs have short (<1 ns) spontaneous emission lifetimes and can easily be monolithically integrated into microcavities to enhance the spontaneous emission rate and generate near-transform-limited pulses [24]–[28]. Recently, epitaxial QDs have even been used to generate entangled photon pairs [29], [30]. A major drawback to epitaxial QDs is that they require cryogenic cooling. Our recent results with InGaAs QDs [31] show that this restriction can be relaxed from temperatures that require cooling with liquid helium (4 K) to the more easily achieved temperatures accessible with liquid nitrogen (77 K).

Although the development of single photon sources is still in its infancy, single photon detectors have been commercially available for many years. The most common single photon detectors are photomultiplier tubes (PMTs) and silicon and InGaAs avalanche photodiodes (APDs). However, no commercial device meets all of the desired specifications of an ideal single photon detector, including low dark count rate, high quantum efficiency, no afterpulsing, and wide spectral bandwidth. Another important characteristic is the timing jitter, which is the pulse-to-pulse variation in the time delay between the photon absorption and the electrical pulse output. A detector with lower timing jitter can be used to achieve higher timing resolution in TCSPC, increased bit rates in QKD, or improved spatial resolution in time-of-flight applications such as LIDAR and PICA.

Silicon APDs are the most common detector for wavelengths from about 400–1050 nm, with high detection efficiency (DE) (up to 76% at 700 nm) and low dark counts (~50–100 Hz) [32]. The lowest timing jitter reported is 20-ps full-width at half-maximum (FWHM) [33], but typical values for the commercial units are two to ten times higher. In addition, the narrow central peak of a commercial device's temporal response function is nearly always followed by a long exponential tail [34]; this non-Gaussian response complicates the data analysis. For single photon detection of wavelengths >1050 nm, InGaAs APDs were until recently the only real option [34]–[37]. InGaAs devices generally have very high dark count rates—as low as 1 kHz, but typically >10 kHz—and thus are almost always operated in a gated mode [34], [36], which requires knowing the expected photon arrival time to within a few nanoseconds. Furthermore, the quantum efficiency of InGaAs APDs is relatively low (~20%), and they must be operated with a long deadtime to prevent afterpulsing. Timing jitter below 300 ps can be achieved, but at the cost of even higher dark count rates [37].

To address some of the shortcomings of the commercial detectors, alternatives are under development at various research laboratories. For example, superconducting transition edge sensors (TESs) [38], [39] have detection efficiencies up to 89% and virtually zero dark counts. TESs also have a demonstrated ability to resolve the number of photons in a pulse of light, a feature no commercial detector can yet offer and an important component of many quantum information schemes. As another example, superconducting single photon detectors (SSPDs) have been operated at up to 1 GHz count rates with low dark count probability and timing jitter as low as 18 ps [40]–[43]. Furthermore, both TESs and SSPDs offer detection capability well into the infrared.

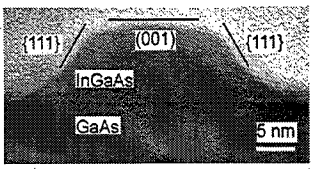

Fig. 1. Transmission electron micrograph of an InGaAs QD grown on a GaAs substrate. Unlike the QDs used in the optical measurements, this dot has not been capped with GaAs.

In this paper, we review some of our recent progress on epitaxial InGaAs QD single photon sources and SSPDs [31], [44], [45]. In Section II, we outline experimental techniques. In Section III, we discuss emission from a single InGaAs QD at temperatures between 5 and 135 K. We show single photon emission up to 120 K and photon antibunching up to 135 K. Section IV covers QDs embedded in micropillar cavities, showing the effect of the cavity on the QD emission spectrum and demonstrating a decreased spontaneous emission lifetime through the Purcell effect. In Section V, we discuss SSPDs and the details of packaging and implementation into our experimental setup. Section VI describes the use of an SSPD for spontaneous emission lifetime measurements. We show that, unlike conventional Si APDs, the timing jitter profile of the SSPD has a Gaussian shape, offering a significant advantage for measuring lifetimes. We also demonstrate the superconducting detector's utility for a wavelength of 1245 nm, well outside the range of the silicon detectors. Section VII shows the use of the SSPD for single photon source characterization in a Hanbury Brown–Twiss interferometer (HBTI), and a summary follows in Section VIII.

II. Experiment

A. Self-Assembled InGaAs QDs

We grow self-assembled InGaAs QDs using molecular beam epitaxy (MBE), which allows sub-monolayer control of the thickness of a deposited film. InGaAs is deposited on a GaAs substrate, and the large lattice mismatch between these two materials causes strain in the InGaAs film. As the film thickness increases, this strain eventually becomes large enough that small islands form. These islands are capped with GaAs to complete the formation of QDs. Typical dots, like the one shown in Fig. 1, have a height of less than 10 nm and a base diameter of about 25 nm. Careful adjustment of the growth conditions permits growth of a low areal density (approx. 1–10 μm^{-2}) array of InGaAs QDs. Using standard photolithographic and etching techniques, we form pillars of various sizes on the sample to isolate a small number of QDs.

In this paper, we employ two types of QD samples. In the first type, QDs are simply capped with GaAs, and square pillars, ~2-μm-wide, are formed with a wet etch. In the second type, QDs are buried in a vertical microcavity; for these latter dots, the optical cavity is formed by a pair of GaAs/AlAs distributed Bragg reflectors grown above and below the QD layer. A reactive

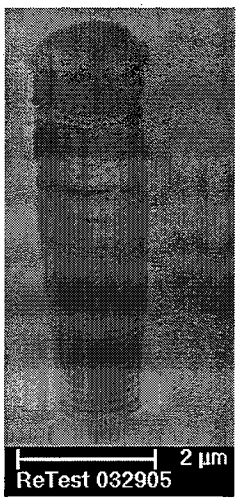

Fig. 2. Scanning electron microscope image of a ~2-μm-diameter micropillar cavity. The top mirror, the QD layer, and most of the bottom mirror are visible.

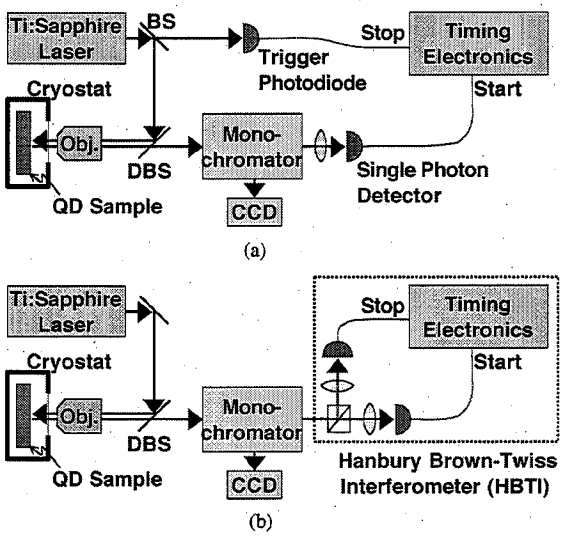

Fig. 3. Experimental geometry. (a) Spectroscopy and TCSPC setup, showing configuration used with timer A. (b) Modified to include HBTI. BS is a beamsplitter, DBS is a dichroic BS, and Obj. is a long-working-distance microscope objective.

ion etch is then used to define the cylindrical micropillars ~6-μm-tall and ~2 μm in diameter, as shown in Fig. 2. The roughness in the pillar sidewalls is due to mask erosion during etching.

B. Photoluminescence (PL) Spectroscopy

The experimental geometry is shown in Fig. 3. The QD samples are placed in a liquid helium-flow cryostat, which provides continuous temperature tuning between room temperature and 4 K. Each sample is excited using a mode-locked, 82 MHz-repetition-rate Ti:Sapphire laser that is tuned to wavelengths between 780 and 850 nm and produces output pulses whose duration ranges from ~200 fs to ~1 ps. These pulses are focused to a spot diameter of ~5 μm in order to excite a single pillar. The PL emitted from the sample is collected by a long-working-distance microscope objective and then focused onto the input slit of either a 0.3 or 0.75 m monochromator. A liquid nitrogen cooled charge-coupled device (CCD) camera is used to record the PL spectrum.

C. TCSPC

We measure the spontaneous emission lifetime of a QD using TCSPC [2] with the experimental arrangement in Fig. 3(a). To perform TCSPC, an internal mirror in the monochromator is flipped to direct the emitted light through an output slit. The resulting spectrally filtered PL is focused onto a single photon detector, which in our case is either a silicon APD or an SSPD.

The heart of TCSPC is the timing electronics, and in this paper, we use two different timers. In timer A, the voltage pulse from the single photon detector starts the timer and the 82-MHz clock signal from the trigger photodiode stops the timer. Operating in this "reverse start–stop" mode ensures that each start is followed by a corresponding stop within 12 ns, which is the time between the laser pulses. This configuration is typical of TCSPC and is necessitated by the relatively long (~95 ns) dead time of the electronics. The time axis is reversed accordingly in the data plots in this paper. Timer B, by contrast, operates in the more intuitive "forward start-stop" mode, where the 82-MHz clock signal starts the timer, and the signal from the single photon detector stops it. Timer A contributes a timing jitter of ~160 ps to the measurements, whereas timer B contributes <30 ps of jitter. Jitter from the electronics should add in quadrature with any jitter from the detector [2].

In both timers, each of the start and stop inputs to the electronics pass through a constant fraction discriminator before engaging a digital time-to-amplitude converter (TAC). The TAC output is fed into a multichannel analyzer, which builds up a histogram of counts versus start–stop time interval (τ). The start rate is kept less than 82 kHz to ensure an average of less than one count per 1000 excitation pulses, preventing a pileup of counts in the early time bins [2]. Under these conditions, the resulting histogram is proportional to the time-resolved PL intensity, giving a direct measure of the spontaneous emission lifetime.

D. Hanbury Brown–Twiss Interferometry

As shown in Fig. 3(b), the experimental setup can be modified so that the monochromator output is directed onto a HBTI [46]. The HBTI consists of a 50/50 beamsplitter cube, two single photon counting detectors, and the timing electronics. A slit at the output of the monochromator is used to adjust the spectral width of the light incident on the HBTI, as appropriate to the QD under study. The timing electronics again produce a histogram of counts versus τ.

For this configuration, in the limit of low count rates, the resulting histogram is proportional to the second-order coherence function [47], [48]

$$g^{(2)}(\tau) = \frac{\langle I(t)I(t+\tau)\rangle}{\langle I(t)\rangle^2} \quad (1)$$

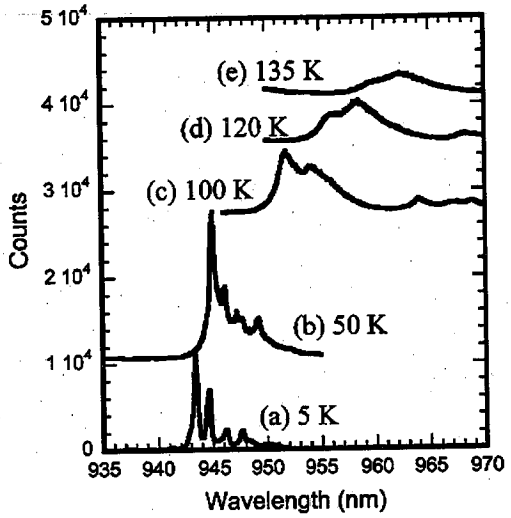

Fig. 4. Temperature-dependent emission spectra from a 2-μm-wide square mesa using a CCD camera with a 10-s integration time. These spectra and the photon correlation measurements shown in Fig. 5 are obtained under identical excitation conditions. The spectra are vertically offset for clarity.

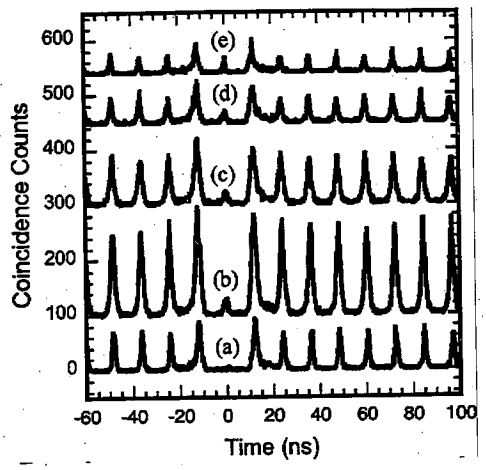

Fig. 5. Coincidence counts measured using the HBTI. The curves are offset from one another for clarity. *Curve labels* correspond to the temperatures shown in Fig. 4.

where I is the intensity and angle brackets indicate an average over time. $g^{(2)}(\tau)$ is also referred to as the second-order intensity correlation. In this low count rate limit, for pulsed excitation with lifetimes much shorter than the pulse repetition interval, the area of the peak at $\tau = 0$ divided by the average area of the surrounding peaks will be equal to the second-order coherence at zero delay, $g^{(2)}(0)$. For a classical Poisson source, such as an attenuated laser pulse train, all peaks are of the same height and $g^{(2)}(0) = 1$. Only a nonclassical source can exhibit antibunching, where the central peak is smaller than the surrounding peaks. Verification of single photon emission further requires $g^{(2)}(0)<0.5$, and an ideal single photon source will have $g^{(2)}(0) = 0$ [48].

III. High-Temperature QD Single Photon Source

The first experimental results we discuss demonstrate the use of a single QD, not embedded in a cavity, as a single photon source. We study QD emission over a temperature range between 5 and 135 K. In these measurements, the Ti:Sapphire laser is tuned to 850 nm, producing ~200-fs pulses, and a 0.3-m monochromator with a 1200 groove/mm grating performs the spectral filtering. Fig. 4 illustrates temperature-dependent PL from a single QD as captured by the CCD camera. Due to the above-bandgap excitation of the GaAs, there are several emission peaks from the QD emission that are associated with excitons, charged excitons, and biexcitons.

To demonstrate single photon emission, we use the HBTI discussed in Section II. For the measurements here, the HBTI detectors are both Si APDs, and the monochromator output slit is adjusted to allow a bandpass of 1.2 nm (2.4 nm at the highest temperature). Fig. 5 shows a histogram of coincidence counts made using the HBTI for each temperature shown in Fig. 4. We show only the peak at zero delay and a few of the adjacent peaks in this figure, but our measurement apparatus allows us to collect data with time separations up to 1115 ns, corresponding to about 90 peaks at the pulse repetition interval of 12 ns. The spontaneous emission lifetime of this QD is about 1 ns, ensuring a high probability that the QD is empty of excited carriers each time a pump pulse arrives.

TABLE I
Temperature-Dependent QD Emission Results

Temperature	Pump Irradiance[a] (W/cm^2)	$g^{(2)}(0)$	f_{ex}
5 K	1.8	0.087 ± 0.009	0.960
50 K	5.3	0.177 ± 0.013	0.735
100 K	16.2	0.260 ± 0.024	0.578
120 K	57.3	0.471 ± 0.067	<0.5
135 K	84.3	0.667 ± 0.063	<0.5

[a]Time averaged pump power density. Any irradiance value in this paper can be converted to a fluence (energy density per pulse) by dividing by the laser repetition rate of 8.2×10^7 s^{-1}.

As shown in Fig. 5, the area of the peak at zero delay is much smaller than the area of any of the other peaks. This is the signature that the photons are emitted one at a time. The measured $g^{(2)}(0)$ value, listed in Table I, is the normalized peak area, which is obtained by dividing the peak area at zero delay by the average area of all the other peaks (including the peaks not shown in the figure). The best results are obtained at 5 K, where $g^{(2)}(0)$ is measured to be 0.087 ± 0.009. This is not surprising, since Fig. 4 shows that the overlap between the exciton peak and the other peaks is smaller at 5 K than it is at any other temperature shown. The second-order intensity correlation at zero delay increases gradually with temperature up to 100 K, and then increases more dramatically up to 135 K. The highest temperature for which $g^{(2)}(0)$ is less than 0.5, the indicator of single photon emission, is 120 K. At the highest temperature of 135 K, the second-order intensity correlation increases to 0.667 ± 0.063, which still indicates nonclassical light emission, but there is no longer evidence of emission from a single quantum system.

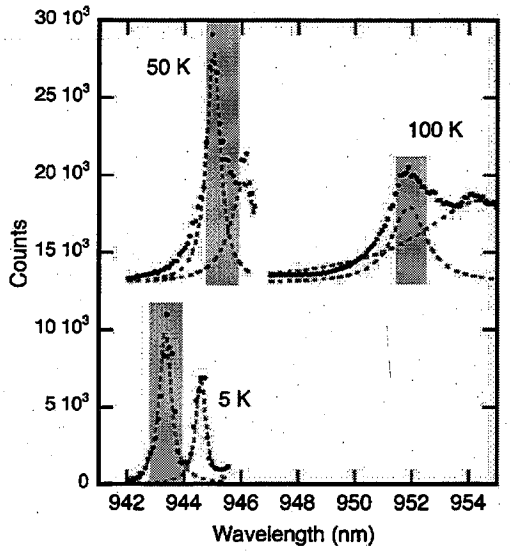

Fig. 6. Measured QD emission spectrum at three temperatures (*solid circles*). Each data set has been fit to a sum of two Lorentzians, and the relative contributions to the fit from the exciton line and the longer wavelength emission line are shown as *dashed curves*. This longer wavelength line is likely emission from a biexciton or charged exciton state. Each *shaded box* represents the monochromator position and spectral bandwidth for the corresponding temperature, illustrating the spectral bandwidth of emission incident on the APDs in the HBTI.

Note that, in Fig. 5, the peaks immediately adjacent to the peak at zero delay are somewhat larger than all of the other peaks, and these adjacent peaks also have tails that do not go completely to zero before subsequent peaks appear. The reason for these features is that a Si APD will occasionally emit photons from the avalanche region after detecting a single photon [49], [50] Inadequate spatial and spectral filtering and imperfect antireflection coatings on optics cause these emitted photons to be detected by the other APD, resulting in false correlations due to this optical crosstalk between the two detectors. We characterize the crosstalk by blocking the QD source and using room lights to trigger the APDs; in our experiment, crosstalk can contribute strongly to the two peaks at $\tau = \pm 12$ ns, weakly to the peaks at ± 24 ns, and little or nothing to the other peaks.

The nonzero value of $g^{(2)}(0)$ is due in part to photons other than those that arise from the uncharged single exciton transition. For the QD studied here, these photons correspond to the peaks at longer wavelengths in the PL spectrum. We are able to accurately fit the spectra for the three lowest temperatures in Fig. 4 to a sum of Lorentzians, as shown in Fig. 6. The linear correlation coefficient R of our fit is greater than 0.95 for each of these three spectra. The fit allows us to determine the width and the center wavelength of the peaks. By using the spectral width (1.2 nm) of the light incident on the HBTI and the fit values for the peaks, we determine the fraction of the counts in the spectra that are due to the uncharged single exciton peak f_{ex}. Fig. 6 shows that the contribution from other transitions is very small at 5 K but increases to be a significant fraction of the single exciton transition at 50 and 100 K. At 50 K, we note that the spectral filter is optimized for maximum count rate rather than minimum $g^{(2)}(0)$; selecting a slightly shorter center wavelength for the spectral filter should decrease $g^{(2)}(0)$ at the expense of longer acquisition time. At 100 K, the single exciton peak is broadened and barely distinguishable from the peak associated with other transitions, which are likely due to biexcitons or charged excitons. For the two highest temperatures, we are unable to obtain a satisfactory fit to the spectra. However, the uncharged single exciton emission peak is smaller than the additional peak at longer wavelengths in these two spectra, so it is likely that the value of f_{ex} is less than 0.50 for these two spectra.

In the present experimental configuration, we have no way to eliminate these other contributions from the stream of photons emitted by the QD. However, it might be possible to obtain a smaller $g^{(2)}(0)$ value at elevated temperatures if the single exciton transition could be excited with greater specificity or if the other contributing transition(s) could be suppressed or filtered. Since the energy difference between the exciton and biexciton transitions varies from one QD to another [51], and since this separation can be tuned with an applied magnetic field [52], it might be possible to isolate a single QD with a detuning that is large enough to minimize the spectral overlap between the exciton and biexciton, even for temperatures above 100 K.

The count rate on the APDs ranges from about 3.5 kHz at 50 K to about 1.1 kHz at 135 K. This includes the mean dark count rates of 65 Hz for one APD and 212 Hz for the other APD. The count rate at 50 K is higher than at 5 K only because the QD is pumped harder at 50 K than at 5 K. When this QD is excited with the same power density at 5 and 50 K, the count rate is about 25% higher at 5 K. However, using a more intense pump leads to some degradation of the intensity correlation function. The total efficiency of the system (defined here as the APD count rate divided by the laser pulse repetition rate) is around 10^{-4}, in part because of the small fraction of emitted photons that are collected by the objective.

There are two reasons why the single InGaAs QD emission rate decreases at higher temperatures, requiring higher pump intensities and subsequently degrading the QD's performance as a single photon source. First, the conduction band offset is relatively small, allowing thermionic emission of electrons out of the QDs into the InGaAs wetting layer. The QD studied here was chosen in part for the separation of its emission from the wetting layer peak. Other QDs with shorter emission wavelengths have also been measured, but these QDs did not perform as well when the temperature increased; this suggests that carrier transfer to the wetting layer is a factor in the degradation of the second-order intensity correlation. Also, optical phonon scattering becomes more pronounced as temperature increases. Using larger QDs (with less quantum confinement energy) or wider bandgap barriers, can mitigate the conduction band offset problem. The phonon scattering problem could be reduced by promoting faster radiative recombination times of the QD excitons by use of a microcavity. Single electron–hole pair injection by electrical means [53] should improve the performance of an InGaAs QD single photon source by eliminating the possibility of charged exciton or biexciton formation.

Despite the complications due to imperfect spectral separation of the exciton line from other emission lines, the results

presented in this section show the promise for high-temperature operation of a single photon source based on self-assembled InGaAs QDs.

IV. QD in a Micropillar Cavity

In contrast to the bare QD used in Section III, we have also embedded QDs in micropillar cavities, which significantly modifies the emission spectra. In the weak coupling regime, the cavity reduces the dot's spontaneous emission lifetime via the Purcell effect [24], [25]. This effect has been observed for epitaxial QDs in micropillar cavities by several research teams [24]–[28]. In addition, the micropillar cavity should increase our collection efficiency, since the pillar effectively "funnels" emitted light into a well-defined near-Gaussian cavity spatial mode. The light in this mode can be efficiently collected by the microscope objective and directed to the detector(s).

Fig. 7 illustrates some of the key changes in the spectrum of a QD when it is embedded in a microcavity. These spectra are acquired with the laser tuned to a center wavelength of 780 nm. Fig. 7(a) shows spectra of a QD without a cavity, and Fig. 7(b) and (c) displays spectra of a QD that was grown inside a cavity. Without a cavity, a weak pump pulse produces a PL spectrum characterized by several discrete lines. These lines result from emission of a small number of QDs in the 2-μm-wide pillar. For a much stronger pump, excited states from all dots in this pillar generate broadband continuum emission that is approximately constant over a bandwidth of several nanometers.

In Fig. 7(b) and (c), the spectra are similar, except that they have been spectrally filtered by the cavity and are shown over a much narrower bandwidth. For a weak pump, only a few emission lines near the cavity resonance are clearly visible. For a strong pump, the near-constant broadband excited state emission is filtered by the cavity transmission profile. As expected for an optical cavity, this transmission profile is well fit by a Lorentzian lineshape. The fit provides a measure of the cavity center wavelength ($\lambda_c = 901.98$ nm) and linewidth ($\Delta\lambda = 0.75$ nm FWHM), yielding a cavity Q of 1200, where $Q = \lambda_c/\Delta\lambda$. Comparison of the two curves in Fig. 7(b) indicates that the brightest single QD line is resonant with the cavity mode at a temperature of 4 K. When the QD temperature is increased to 33 K, Fig. 7(c) shows that this QD line (still the brightest line visible) is redshifted 0.62 nm from its position at 4 K. The cavity, meanwhile, redshifts only 0.20 nm. As a result, this line is detuned by 0.42 nm from the cavity resonance at 33 K.

Spontaneous emission lifetime measurements of this QD for a series of temperatures between 4 and 47 K are plotted in Fig. 8. These measurements are performed using the TCSPC technique described in Section II with a Si APD as the single photon detector and timer A. At 4 K, where the QD line is resonant with the cavity, the spontaneous emission lifetime is ~400 ps. At 47 K, this line is detuned ~1.1 nm from the cavity resonance, and the lifetime is ~640 ps. This rather small spontaneous emission lifetime reduction factor of ~1.6 indicates that we have not yet succeeded in placing a QD at the right spatial location in the pillar, since a cavity Q of 1200 and the small mode volume of the 2-μm-diameter

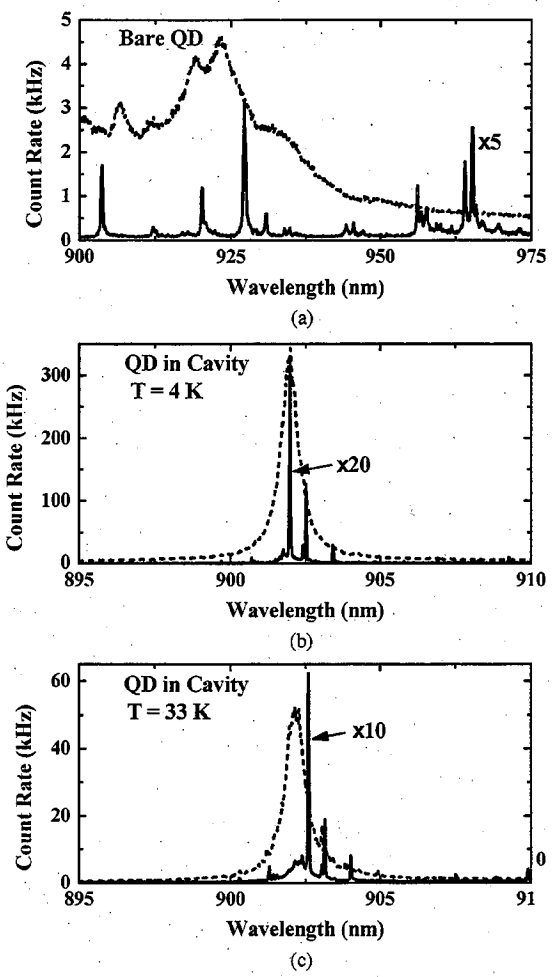

Fig. 7. QD spectra at low and high excitation power, with and without a micropillar cavity. (a) QD in a 2-μm-wide pillar with no vertical cavity at 4 K for average pump irradiance of 3.2 W/cm^2 (*solid curve*) and 10 kW/cm^2 (*dashed curve*). (b) QD in a 2-μm-diameter micropillar cavity at 4 K for 15 W/cm^2 (*solid curve*) and 134 W/cm^2 (*dashed curve*) average pump irradiance. (c) Same conditions as (b), except for a temperature of 33 K.

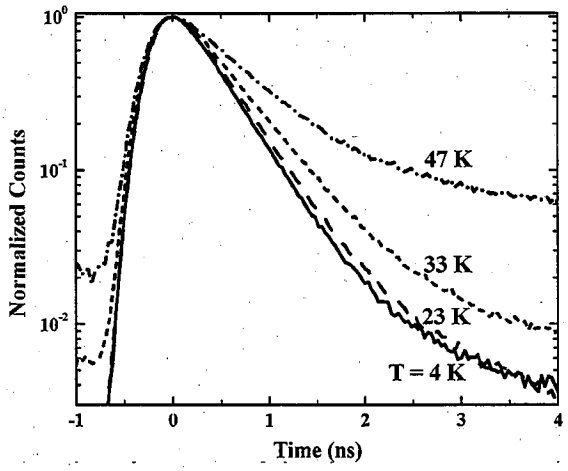

Fig. 8. Spontaneous emission lifetime measurement as a function of temperature for the QD whose spectrum is shown by the *solid curve* in Fig. 7(b) and (c). The cavity-dot detuning is < 0.02 (resolution limited), 0.19, 0.42, and 1.12 nm at 4, 23, 33, and 47 K, respectively.

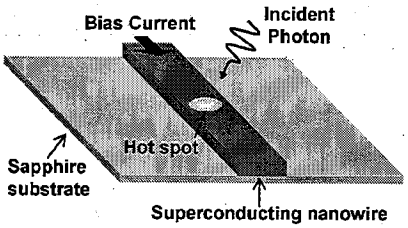

Fig. 9. Principle of operation of a superconducting single photon detector. An absorbed photon creates a resistive hot spot in the wire, resulting in an output voltage pulse.

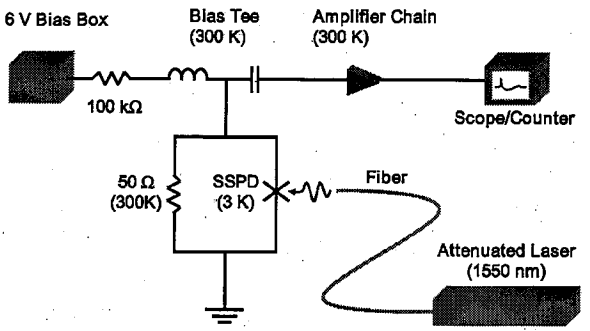

Fig. 10. Schematic of bias and readout circuit.

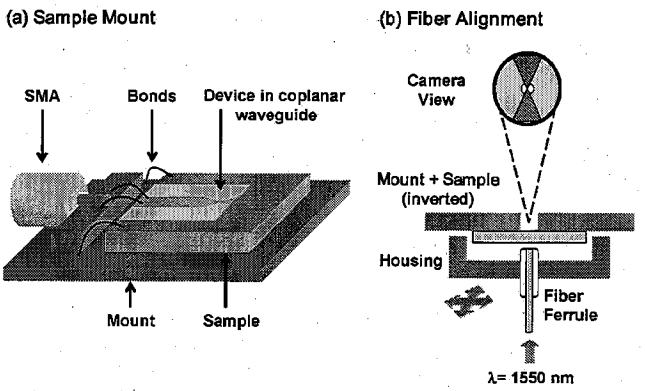

Fig. 11. Drawings. (a) Sample mount. (b) Fiber alignment.

pillar should result in a much stronger Purcell effect [25]. We do find, however, that QDs in cavities tend to produce significantly higher count rates on our detectors than do QDs that are not in cavities, and we use a cavity-embedded QD for the measurements detailed in Section VII.

Note that the decay curves in Fig. 8 are not pure single exponentials, and that the second, long-lived decay component becomes more pronounced as the temperature increases. The latter happens for two reasons: 1) weaker QD emission away from the cavity resonance causes a smaller signal-to-noise ratio and thus a more pronounced background level and 2) the second exponential component is indeed stronger at higher temperatures. Nonexponential decay has previously been observed in QD lifetime measurements, and has been ascribed to multiple sources, some of which can be temperature dependent [54], [55]. A thorough study of the nature of these decays is outside the scope of the present work; nevertheless, it is clear from Fig. 8 that the effective lifetime of the exciton increases as the detuning from the cavity resonance increases.

V. SSPDs

Now that we have discussed our QD single photon sources in detail, we describe the SSPDs that we use to characterize these sources. Each SSPD device is a narrow, superconducting niobium nitride (NbN) wire embedded in a 50-Ω transmission line. The superconducting track is current biased just below its critical current I_C. When this wire absorbs a photon, it momentarily creates a nonsuperconducting hot spot, as shown in Fig. 9. As a result, a small voltage is developed briefly across this resistive section of the track, causing a high-speed voltage pulse to propagate along the transmission line [56]–[59]. The early devices, consisting of a single straight NbN wire, suffered from low DE [40], owing to the difficulty of coupling light to such a small detector area. The SSPDs used here boost DE through a 100-nm-width meander line with 200-nm pitch, covering a 10 μm $\times$10 μm area [41].

Since the superconducting detector must be operated at temperatures near 4 K, we have packaged the device in a practical, cryogen-free system using a commercially available cryocooler [44]. In this system, a low-noise current source is used to bias the detector, and commercial, room temperature RF amplifiers with adequate bandwidth and sufficiently low noise figure amplify the pulses generated by the detector, as shown in Fig. 10. The amplified voltage pulses can be observed on an oscilloscope, read out on a digital counter, or converted into digital logic pulses.

Light is coupled to the detector by a method previously developed at the National Institute of Standards and Technology (NIST) for transition edge sensor single photon detectors [38], [39], as shown in Fig. 11. Each detector is mounted on a small metal block. Aluminum wirebonds connect the on-chip coplanar waveguide to a subminiature A (SMA) connector. High-speed coaxial cables that are heat-sunk at 2.9 and 40 K conduct the signal from the detector to room temperature. A polished fiber is held in a second metal block positioned over the chip carrier. The fiber in the ferrule holder is aligned over the detector by viewing the transmission of fiber-coupled 1550-nm light through the chip with an infrared microscope. The position of the fiber/fiber holder is adjusted such that the detector blocks the light. This method allows alignment of the fiber to the chip with a precision of a few micrometers. Single mode optical fiber enters the cryostat via an epoxy feed through.

Stable operation (constant DE and dark count rate) of the SSPD requires stable operating temperatures [40]–[43]. For the SSPD system, we use a compact, closed-cycle, cryogen-free, Gifford–McMahon-type cryocooler [60]. The refrigerator has sufficient capacity to cool a number of detectors simultaneously to 2.9 K. However, the cold head temperature fluctuates approximately $\pm$0.3 K peak-to-peak at 1.2 Hz. We passively stabilize the temperature of the detector assembly by weakly

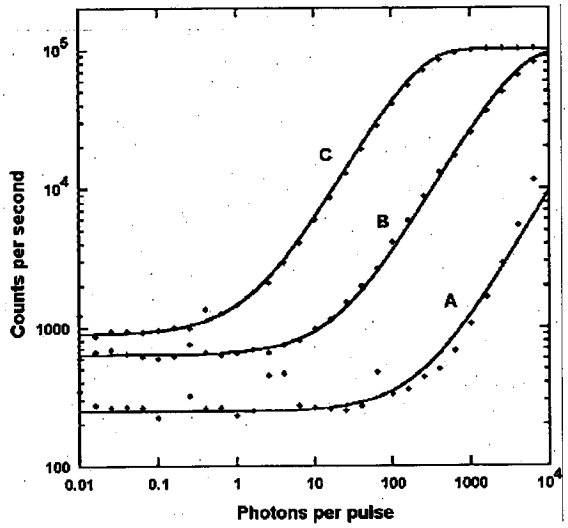

Fig. 12. Determination of SSPD efficiency and dark count rate for three values of bias current. The laser wavelength is 1550 nm and the repetition rate is 100 kHz. For data sets A, B, and C, I_{Bias} is set at 68%, 80%, and 94% of I_C, respectively. The *solid curves* are fits to the equation given in (2) for dark count rate D and DE η. The fits yield values of $D = 250$ Hz and $\eta = 8 \times 10^{-6}$ for data set A, $D = 640$ Hz and $\eta = 2 \times 10^{-4}$ for B, and $D = 900$ Hz and $\eta = 5 \times 10^{-3}$ for C.

coupling the detector stage to the cold stage; this reduces the fluctuations to a few millikelvins.

We determine the system DE at 1550 nm using an attenuated, pulsed telecommunications laser. A conventional power meter is used to measure the average power output from the pulsed laser. Given the power, pulse repetition frequency ($f = 100$ kHz), and wavelength, we can estimate the mean number of photons per pulse μ. For a given bias current I_{Bias}, the total count rate R is recorded as a function of μ. The single photon DE η, coupled to a source with a Poisson photon number distribution (such as a laser), can be extracted by fitting to the relation

$$R \approx D + f(1 - e^{-\eta\mu}) \tag{2}$$

where D is the dark count rate. Fig. 12 shows the results of this DE measurement procedure for three values of bias current, along with fits to (2). For a single-photon counting detector, when $\eta\mu \ll 1$, R should increase linearly with μ, since (2) reduces to $R \approx D + f\eta\mu$. This linear dependence on μ is evident in the excellent agreement between the data and fits in Fig. 12. By contrast, if the detector were counting multi-photon events, rather than single-photon events, then R would have a superlinear dependence on μ.

Fig. 13 shows the system DE versus dark count rate for a series of bias currents at two wavelengths: 902 and 1550 nm. The tradeoff between efficiency and dark counts is evident in this figure, as a high bias current yields a large DE, but at the expense of elevated dark counts. Therefore, the optimum bias current for a given measurement depends on the source wavelength, light level, and other experimental details. Intrinsic detection efficiencies of up to 10% for the same type of detectors at 1550 nm have been reported [43]. For this packaged,

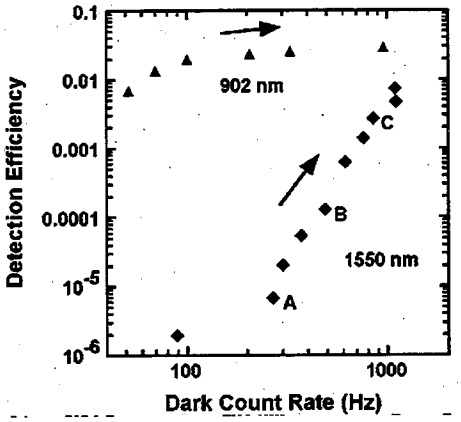

Fig. 13. SSPD system DE versus dark counts at 902 (*triangles*) and 1550 nm (*diamonds*). The *arrows* indicate the direction of increasing bias towards I_C. The data cover the approximate range in I_{Bias} from 60% to 95% I_C. The labels A, B, and C indicate the values determined from the corresponding data sets in Fig. 12.

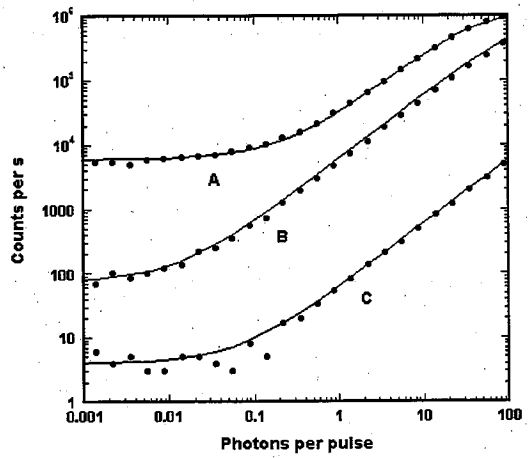

Fig. 14. Determination of efficiency and dark count rate of a second SSPD. The laser wavelength is again 1550 nm, but here the repetition rate is increased to 1 MHz. For data sets A, B, and C, I_{Bias} is set at 96%, 82%, and 65% of I_C, respectively. The *solid curves* are fits to the equation given in (2) for dark count rate D and DE η. The fits yield values of $D = 6$ kHz and $\eta = 2.7 \times 10^{-2}$ for data set A, $D = 75$ Hz and $\eta = 6 \times 10^{-3}$ for B, and $D = 4.5$ Hz and $\eta = 6 \times 10^{-5}$ for C.

fiber-coupled detector, the maximum observed DE at 1550 nm is ~1%.

At 902 nm, we find the SSPD system DE by fixing the PL light level and comparing the SSPD's count rate to the count rate on a Si APD with a known DE. As Fig. 13 shows, the maximum DE of 3% and maximum dark count rate of 1 kHz are obtained for I_{Bias} near I_C. Below I_C, the dark count rate falls more rapidly than the DE, allowing us to achieve a 2% DE at ~100-Hz dark count rate. The increase in DE at 902 nm compared to 1550 nm is due primarily to the higher photon energy at 902 nm.

Another demonstration of single-photon counting is presented in Fig. 14, which shows efficiency and dark count measurements on a second SSPD. Here, we use the same configuration as for Fig. 12, except with a higher laser repetition frequency of $f = 1$ MHz. For $I_{\mathrm{Bias}} = 0.82 I_C$ (data set B), even

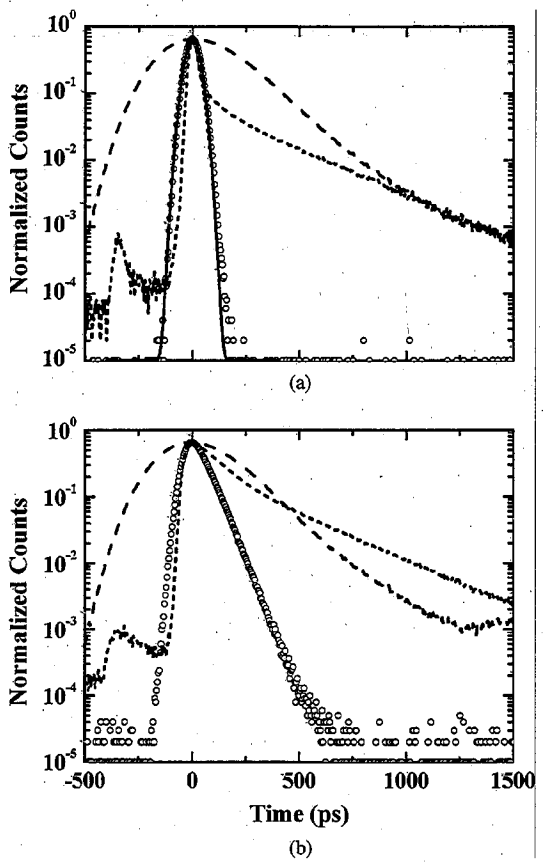

Fig. 15. (a) Instrument response functions of three detectors: SSPD (*open circles*), conventional Si APD (*dashed curve*), and fast Si APD (*dotted curve*). The *solid curve* is a Gaussian fit to the measured SSPD response function. (b) Lifetime measurement of QW emission at 935 nm with these three detectors. The time axes in (a) and (b) are identical.

with 0.1 photons per laser pulse, nearly 90% of the counts from the detector are signal counts.

VI. Lifetime Measurements Using an SSPD

To compare the performance of the SSPD with the conventional silicon APDs, we insert each detector into our TCSPC setup and use timer B. First, we characterize the timing jitter by measuring each detector's temporal instrument response function (IRF). We then measure the spontaneous emission lifetimes of two semiconductor quantum wells (QWs) that emit in the infrared, including one QW that emits at a wavelength of 1245 nm, well outside the range of silicon detectors.

For the measurements in this section, we again use the Ti:Sapphire laser, which is tuned to 780 nm and produces ~ 1 ps pulses. To measure the IRF of a detector, we tune the monochromator to 780 nm to pass only the heavily attenuated laser pulse train. Results are shown in Fig. 15(a). The SSPD's response is fit well—over nearly *five decades* of dynamic range—by a Gaussian with a FWHM of 71 ps. Averaging several measurements yields a timing jitter of 68 ± 3 ps FWHM. This jitter is independent of the count rate between 50 Hz and 1 MHz. Note that timing jitter as low as 18 ps has been reported for similar SSPD devices; however, these previous measurements were done in a regime where the detector produced a voltage pulse for *every* incident laser pulse [42], [43]. Here, by contrast, we report timing jitter measurements for the much lower count rates required for TCSPC. Differences in our device, amplifier, or timing electronics may also contribute to this discrepancy with previous work. Also note that the IRFs measured here include time jitter from the electronics (here <30 ps), which should add in quadrature with any jitter from the detector [2].

For comparison, Fig. 15(a) also shows the measured IRFs of a conventional silicon APD (FWHM $\approx$ 400 ps) and a fast Si APD (FWHM $\approx$ 40 ps). Although the fast APD has a narrow main peak, it also has an exponential tail that persists for several hundred picoseconds. This diffusion tail, which is typical of APDs, is caused by the slow diffusion of photoexcited carriers from the neutral region into the high-field region of the device [34]. The relative magnitudes of the main peak and tail—and thus the shape of the total IRF—are strongly wavelength dependent, further complicating the analysis of measured decay curves [34], [61].

The advantage of the SSPD over the Si detectors is evident in Fig. 15(b), which shows lifetime measurements of a GaAs/InGaAs QW (QW1). This sample has an emission peak at 935 nm, and was chosen for its relatively short lifetime. Only the SSPD-measured lifetime clearly shows a clean single exponential decay, even without deconvolving the IRF. Although the SSPD has a fairly low DE ($\sim$2% at 900 nm including fiber coupling losses), its low dark count rate (here, $\sim$20–40 Hz) allows measurements with several decades of dynamic range simply by increasing the integration time—although here it is still under three minutes. In addition, identification of multi-exponential processes should be far more straightforward with the SSPD's Gaussian-shaped IRF than with the multi-component response of either Si APD.

Fig. 16(a) plots the SSPD IRF and decay data from Fig. 15, along with a fit. This fit is the measured IRF convolved with an exponential having a 58-ps decay constant. Fig. 16(b) shows similar data for a GaAs/GaInNAs double QW (QW2) emitting at 1245 nm: here the fit has a decay time of 333 ps. The data in Fig. 16(b) could not have been acquired using either of the Si APDs, since this wavelength is well outside the photosensitive range of silicon.

Table II summarizes the performance of these three detectors. The IRF FWHM of the two Si APDs are consistent with the manufacturer specifications, assuming $\sim$20-ps jitter contribution from our TCSPC electronics. The SSPD's response function has a full-width at one one-hundredth maximum (FW(1/100)M) of $\sim$190 ps, and a FW(1/1000)M of $\sim$240 ps. Clearly, these widths are much narrower than the corresponding widths for either Si APD studied here. The fastest available Si APDs and microchannel plate PMTs have IRFs between 20 and 30 ps FWHM [2]. However, these IRFs are typically plagued by long diffusion tails like those visible in Fig. 15(a) [34], [62]. Dual-junction Si APDs offer improved temporal response shapes with FW(1/100)M and FW(1/1000)M values that are similar to the SSPD studied here [34], [62]. Nevertheless, as these dual-junction devices rely on silicon, they are not sensitive to wavelengths beyond 1 μm.

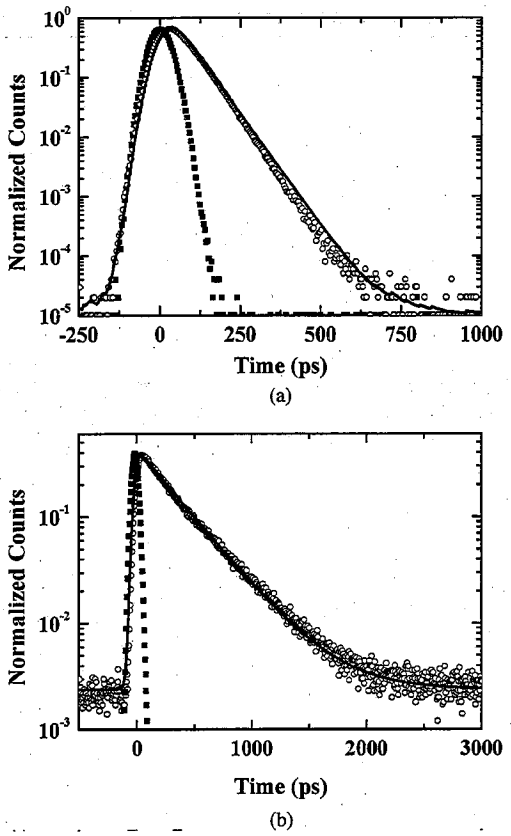

Fig. 16. Lifetime measurements for QWs using an SSPD: IRF (*solid squares*), measured decay (*open circles*), and fit (*solid curve*). (a) QW1 at 935 nm. (b) QW2 at 1245 nm.

TABLE II
DETECTOR PERFORMANCE

	Conventional Si APD	Fast Si APD	SSPD
IRF FWHM	400 ps	40 ps	68 ps
IRF FW(1/100)M	1282 ps	787 ps	190 ps
IRF FW(1/1000)M	1948 ps	1531 ps	236 ps
Dark count rate	100 Hz	50 Hz	100 Hz
DE @ 902 nm	38 % [a]	5 % [a]	2 % [b]
DE @ 1550 nm	n/a	n/a	1% [b,c]
Count rate in HBTI measurement	13 kHz	n/a	600 Hz

[a]Manufacturer specification [b]Coupling losses included
[c]With 1 kHz dark count rate

VII. SSPD FOR SINGLE PHOTON SOURCE CHARACTERIZATION

Next, we demonstrate that the SSPD is sensitive enough to characterize the emission of a single QD. First, we measure the spontaneous emission lifetime; then, we replace one of the Si APDs in the HBTI with an SSPD to measure the second-order intensity correlation function and verify single photon emission.

Fig. 17 shows the spectrum of a QD embedded in a 2 μm-wide micropillar cavity at a temperature of 30 K for a strong and weak pump. Here, we use a 0.75 m monochromator with a 1200 groove/mm grating, and the Ti:Sapphire laser again produces $\sim$1-ps pulses at 780 nm. As discussed in Section IV, low-pump-power emission is dominated by a single QD line at

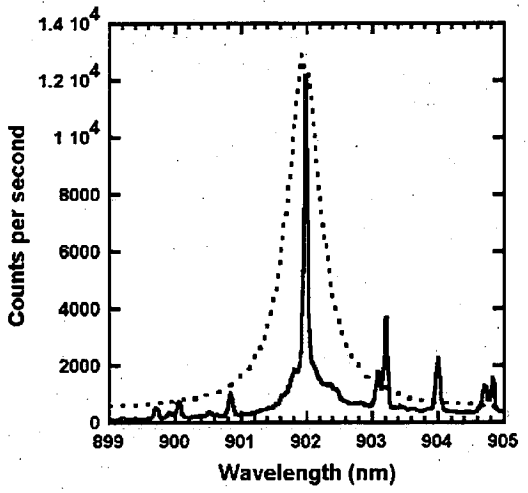

Fig. 17. Emission spectra of cavity-embedded QD at low pump irradiance (23 W/cm^2, *solid trace*) and high pump irradiance (206 W/cm^2, *dotted trace*, magnitude divided by a factor of 50). The QD temperature is 30 K, and the laser is tuned to a central wavelength of 780 nm and emits $\sim$1-ps pulses.

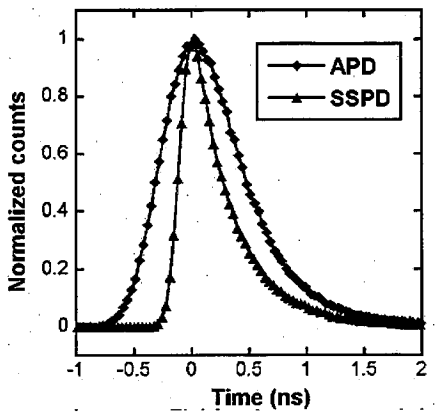

Fig. 18. Time-resolved measurements of spontaneous emission lifetime of a QD emitting at 902 nm. The *triangles* are data acquired with an SSPD, the *diamonds* with a conventional Si APD. These data are taken under the same excitation conditions as the 23 W/cm^2 pump spectrum in Fig. 17.

$\sim$902nm, with other emission lines from this dot or other dots in the same pillar visible as weaker surrounding peaks. At high pump power, the Lorentzian-shaped cavity mode is visible. The cavity mode is also centered at $\sim$902 nm and has a FWHM of $\sim$0.6 nm. In the remainder of this section, we study this QD under the same experimental conditions as the low power spectrum shown in Fig. 17, with the monochromator tuned to pass only the emission line at $\sim$902 nm that is resonant with the micropillar cavity mode.

Fig. 18 shows the spontaneous emission lifetime of this dot for these excitation conditions that we measure using both the SSPD and the slower of the two Si APDs discussed in the previous section. Because timer A (jitter $\sim$160 ps) is used for these measurements, the SSPD IRF here is degraded to $\sim$170 ps FWHM. Nevertheless, this IRF is significantly narrower than the IRF of the Si APD (here $\sim$550 ps). As a result, the rising edge of

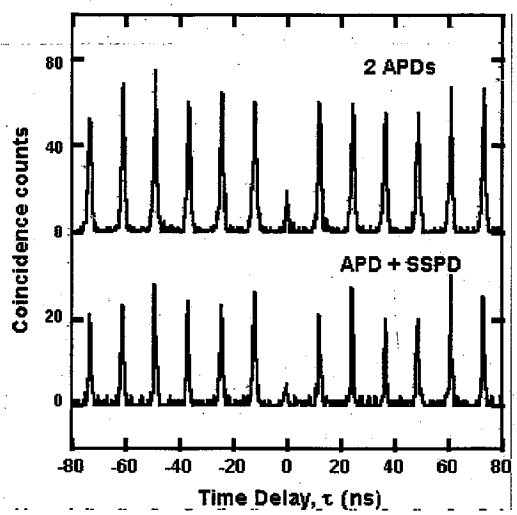

Fig. 19. Coincidence counts as a function of start-stop time delay for the InGaAs QD single photon source measured with the HBTI using two APDs (*top curve*) and one APD and one SSPD (*bottom curve*).

the time-resolved PL is much sharper when measured with the SSPD than with the APD. The rising edge in the emission itself is dominated by the carrier capture time, which is typically under 50 ps [63]; a sufficiently fast SSPD paired with fast electronics could permit one to fully resolve this rising edge, allowing a measure of this capture time for a single dot. Fitting each data set to the convolution of the appropriate IRF with a single exponential yields a decay time of 370 ps for each measured curve. These fits are shown as solid lines in Fig. 18.

To measure the second-order intensity correlation of this QD emission line, we again use the HBTI discussed in Section II, but this time with one output of the beamspitter (BS) focused onto a Si APD and the other BS output coupled to a single mode fiber whose output is directed to the SSPD. Under these conditions, we obtain the coincidence histogram shown as the bottom trace in Fig. 19, where we find $g^{(2)}(0) = 0.24 \pm 0.03$. This indicates a four-fold reduction in the probability of generating more than one photon in a pulse relative to a classical Poisson source of the same intensity. We repeat this measurement using a Si APD in each arm of the HBTI (top trace in Fig. 19), finding excellent agreement with $g^{(2)}(0) = 0.24 \pm 0.05$. The width of the peaks in each histogram is determined in part by the detector IRFs, but mostly by the QD spontaneous emission lifetime. As a result, the peaks in the SSPD/APD configuration are 17% narrower than in the double APD configuration, owing to the lower jitter of the SSPD. If a second SSPD detector were available, we would expect a 40% narrowing of the peaks.

Detector count rates for this measurement are shown in the last row of Table II. The 2% DE of the SSPD system for the bias conditions used here is deduced from the count rate relative to the Si APD. Fiber coupling losses are included in the SSPD system DE—thus, the 2% value in the table represents the lower limit of the DE of the detector itself at $\lambda = 902$ nm. Losses within our SSPD system include free space to fiber outside the cryostat and fiber to SSPD inside the cryostat. Since the optical coupling efficiency into the SSPD system may be as low as 20%, the true DE of the SSPD at 902 nm may be as high as 10%. If a second SSPD detector were available, we could perform this HBTI measurement with two SSPDs, which would be of particular interest for characterizing single photon sources for wavelengths longer than 1 μm. Since single photon sources at telecom wavelengths [64]–[66] are a key element in fiber-based QKD, these SSPDs should prove an important tool in future characterization of infrared single photon emitters.

VIII. Summary

In this paper, we have demonstrated single photon emission from a single InGaAs QD at temperatures up to 120 K, and photon antibunching up to 135 K. These measurements indicate the potential for sources of single photons based on InGaAs QDs that operate at high temperature. We have also shown that embedding a QD in a micropillar cavity can alter the emission by spectrally filtering the PL and by reducing the spontaneous emission lifetime.

In addition, we have demonstrated the use of an SSPD in a TCSPC measurement system. In contrast to the conventional silicon APDs, this detector has a Gaussian temporal response, which is clearly advantageous for determining short lifetimes or analyzing multi-exponential decays. We have also used this superconducting detector to characterize a QD single photon source at 902 nm. The reduced jitter and high signal-to-noise of the SSPD allow us to make improved measurements of carrier lifetime. Unlike Si APDs, this detector retains single photon counting capability into the infrared, making it a promising candidate for single photon source characterization at conventional telecommunications wavelengths. With these advantages, superconducting detectors like this one should have many practical uses, from characterizing weakly emitting materials and fiber-based QKD to a host of other applications requiring high time resolution and single photon sensitivity in the infrared region of the spectrum.

Acknowledgment

The authors would like to thank N. Bergren, J. Berry, C. Elliot, E. Gansen, S. Gruber, T. Harvey, A. Miller, A. Norman, K. Silverman, M. Su, and H. Yeh for their contributions to this work; G. Gol'tsman for providing the superconducting detectors; and J. Gupta for supplying sample QW2. Preparation of the microcavity was performed with the assistance of the UCSB Nanofabrication facility, a member of the NSF-funded National Nanofabrication Infrastructure Network.

References

[1] N. Gisin, G. Ribordy, W. Tittel, and H. Zbinden, "Quantum Cryptography," *Rev. Mod. Phys.*, vol. 74, pp. 145–196, Jan. 2002.

[2] W. Becker, *Advanced Time-Correlated Single Photon Counting Techniques* (Springer Series in Chemical Physics) vol. 81, Berlin, Germany: Springer, 2005.

[3] P. H. Eberhard, "Background level and counter efficiencies required for a loophole-free Einstein–Podolsky–Rosen experiment," *Phys. Rev. A, Gen. Phys.*, vol. 47, pp. R747–R750, Feb. 1993.

[4] M. W. Mitchell, J. S. Lundeen, and A. M. Steinberg, "Super-resolving phase measurements with a multiphoton entangled state," *Nature*, vol. 429, pp. 161–164, May 2004.

[5] P. Walther, J. -W. Pan, M. Aspelmeyer, R. Ursin, S. Gasparoni, and A. Zeilinger, "De Broglie wavelength of a non-local four-photon state," *Nature*, vol. 429, pp. 158–161, May 2004.

[6] Z. Zhao, Y. -A. Chen, A. -N. Zhang, T. Yang, H. J. Briegel, and J.-W. Pan, "Experimental demonstration of five-photon entanglement and open-destination teleportation," *Nature*, vol. 430, pp. 54–58, Jul. 2004.

[7] H. S. Eisenberg, G. Khoury, G. A. Durkin, C. Simon, and D. Bouwmeester, "Quantum entanglement of a large number of photons," *Phys. Rev. Lett.*, vol. 93, pp. 193901-1–193901-4, Nov. 2004.

[8] W. C. Priedhorsky, R. C. Smith, and C. Ho, "Laser ranging and mapping with a photon-counting detector," *Appl. Opt.*, vol. 35, pp. 441–452, Jan. 1996.

[9] J. C. Tsang, J. A. Kash, and D. P. Vallet, "Time-resolved optical characterization of electrical activity in integrated circuits," *Proc. IEEE*, vol. 88, no. 9, pp. 1440–1459, Sep. 2000.

[10] B. Lounis and M. Orrit, "Single-photon sources," *Rep. Prog. Phys.*, vol. 68, pp. 1129–1179, Apr. 2005.

[11] A. Kuhn, M. Hennrich, and G. Rempe, "Deterministic single-photon source for distributed quantum networking," *Phys. Rev. Lett.*, vol. 89, pp. 067901-1–067901-4, Aug. 2002.

[12] J. McKeever, A. Boca, A. D. Boozer, R. Miller, J. R. Buck, A. Kuzmich, and H. J. Kimble, "Deterministic generation of single photons from one atom trapped in a cavity," *Science*, vol. 303, pp. 1992–1994, Mar. 2004.

[13] M. Keller, B. Lange, K. Hayasaka, W. Lange, and H. Walther, "Continuous generation of single photons with controlled waveform in an ion-trap cavity system," *Nature*, vol. 431, pp. 1075–1078, Oct. 2004.

[14] T. Legero, T. Wilk, M. Hennrich, G. Rempe, and A. Kuhn, "Quantum beat of two single photons," *Phys. Rev. Lett.*, vol. 93, pp. 070503-1–070503-4, Aug. 2004.

[15] A. Aspect, J. Dalibard, and G. Roger, "Experimental tests of Bell's inequalities using time-varying analyzers," *Phys. Rev. Lett.*, vol. 49, pp. 1804–1807, Dec. 1982.

[16] P. Michler, A. Kiraz, C. Becher, W. V. Schoenfeld, P. M. Petroff, L. D. Zhang, E. Hu, and A. Imamoğlu, "A quantum dot single photon turnstile device," *Science*, vol. 290, pp. 2282–2285, Dec. 2000.

[17] C. Santori, M. Pelton, G. Solomon, Y. Dale, and Y. Yamamoto, "Triggered single photons from a quantum dot," *Phys. Rev. Lett.*, vol. 86, pp. 1502–1505, Feb. 2001.

[18] K. Sebald, P. Michler, T. Passow, D. Hommel, G. Bacher, and A. Forchel, "Single-photon emission of CdSe quantum dots at temperatures up to 200 K," *Appl. Phys. Lett.*, vol. 81, pp. 2920–2922, Oct. 2002.

[19] P. Michler, A. Imamoğlu, M. D. Mason, P. J. Carson, G. F. Strouse, and S. K. Buratto, "Quantum correlation among photons from a single quantum dot at room temperature," *Nature*, vol. 406, pp. 968–970, Aug. 2000.

[20] J. Hours, S. Varoutsis, M. Gallart, J. Bloch, I. Robert-Philip, A. Cavanna, I. Abram, F. Laruelle, and J. M. Gérard, "Single photon emission from individual GaAs quantum dots," *Appl. Phys. Lett.*, vol. 82, pp. 2206–2208, Apr. 2003.

[21] B. Lounis and W. E. Moerner, "Single photons on demand from a single molecule at room temperature," *Nature*, vol. 407, pp. 491–493, Sep. 2000.

[22] A. Beveratos, S. Kühn, R. Brouri, T. Gacoin, J. -P. Poizat, and P. Grangier, "Room temperature stable single-photon source," *Eur. Phys. J. D*, vol. 18, pp. 191–196, Feb. 2002.

[23] E. Knill, R. Laflamme, and G. J. Milburn, "A scheme for efficient quantum computation with linear optics," *Nature*, vol. 409, pp. 46–52, Jan. 2001.

[24] J. M. Gérard and B. Gayral, "Strong Purcell effect for InAs quantum boxes in three-dimensional solid-state microcavities," *J. Lightw. Technol.*, vol. 17, no. 11, pp. 2089–2095, Nov. 1999.

[25] J. M. Gérard, "Solid-state cavity-quantum electrodynamics with self-assembled quantum dots," *Top. Appl. Phys.*, vol. 90, pp. 269–314, 2003.

[26] C. Santori, D. Fattal, J. Vučković, G. S. Solomon, and Y. Yamamoto, "Indistinguishable photons from a single-photon device," *Nature*, vol. 419, pp. 594–597, Oct. 2002.

[27] S. Varoutsis, S. Laurent, P. Kramper, A. Lemaître, I. Sagnes, I. Robert-Philip, and I. Abram, "Restoration of photon indistinguishability in the emission of a semiconductor quantum dot," *Phys. Rev. B, Condens. Matter*, vol. 72, pp. 041303-1–041303-4, Jul. 2005.

[28] D. C. Unitt, A. J. Bennett, P. Atkinson, D. A. Ritchie, and A. J. Shields, "Polarization control of quantum dot single-photon sources via a dipole-dependent Purcell effect," *Phys. Rev. B, Condens. Matter*, vol. 72, pp. 033318-1–033318-4, Jul. 2005.

[29] R. J. Young, R. M. Stevenson, P. Atkinson, K. Cooper, D. A. Ritchie, and A. J. Shields, "Improved fidelity of triggered entangled photons from single quantum dots," *New J. Phys.*, vol. 8, p. 29, Feb. 2006.

[30] N. Akopian, N. H. Lindner, E. Poem, Y. Berlatzky, J. Avron, D. Gershoni, B. D. Gerardot, and P. M. Petroff, "Entangled photon pairs from semiconductor quantum dots," *Phys. Rev. Lett.*, vol. 96, p. 130501, Apr. 2006.

[31] R. P. Mirin, "Photon antibunching at high temperature from a single InGaAs/GaAs quantum dot," *Appl. Phys. Lett.*, vol. 84, pp. 1260–1262, Feb. 2004.

[32] P. G. Kwiat, A. M. Steinberg, R. Y. Chiao, P. H. Eberhard, and M. D. Petroff, "High-efficiency single-photon detectors," *Phys. Rev. A, Gen. Phys.*, vol. 48, pp. R867–R870, Aug. 1993.

[33] S. Cova, A. Lacaita, M. Ghioni, G. Ripamonti, and T. A. Louis, "20-ps timing resolution with single-photon avalanche diodes," *Rev. Sci. Instrum.*, vol. 60, pp. 1104–1110, Jun. 1989.

[34] S. Cova, M. Ghioni, A. Lotito, I. Rech, and F. Zappa, "Evolution and prospects for single-photon avalanche diodes and quenching circuits," *J. Mod. Opt.*, vol. 51, pp. 1267–1288, Jun. 2004.

[35] J. G. Rarity, T. E. Wall, K. D. Ridley, P. C. M. Owens, and P. R. Tapster, "Single-photon counting for the 1300–1600-nm range by use of Peltier-cooled and passively quenched InGaAs avalanche photodiodes," *Appl. Opt.*, vol. 39, pp. 6746–6753, Dec. 2000.

[36] G. Ribordy, N. Gisin, O. Guinnard, D. Stucki, M. Wegmuller, and H. Zbinden, "Photon counting at telecom wavelengths with commercial InGaAs/InP avalanche photodiodes: Current performance," *J. Mod. Opt.*, vol. 51, pp. 1381–1398, Jun. 2004.

[37] J. S. Vickers, R. Ispasoiu, D. Cotton, J. Frank, B. Lee, and S. Kasapi, "Time-resolved photon counting system based on a Geiger-mode InGaAs/InP APD and a solid immersion lens," in *Proc. 16th Annu. Meeting IEEE LEOS*, vol. 2, 2003, pp. 600–601.

[38] D. Rosenberg, A. E. Lita, A. J. Miller, S. W. Nam, and R. E. Schwall, "Performance of photon-number resolving transition-edge sensors with integrated 1550 nm resonant cavities," *IEEE Trans. Appl. Supercond.*, vol. 15, no. 2, pp. 575–578, Jun. 2005.

[39] D. Rosenberg, A. E. Lita, A. J. Miller, and S. W. Nam, "Noise-free high-efficiency photon-number-resolving detectors," *Phys. Rev. A, Gen. Phys.*, vol. 71, pp. 061803-1–061803-4, Jun. 2005.

[40] G. N. Gol'tsman, O. Okunev, G. Chulkova, A. Lipatov, A. Semenov, K. Smirnov, B. Voronov, A. Dzardanov, C. Williams, and R. Sobolewski, "Picosecond superconducting single-photon optical detector," *Appl. Phys. Lett.*, vol. 79, pp. 705–707, Aug. 2001.

[41] A. Verevkin, J. Zhang, R. Sobolewski, A. Lipatov, O. Okunev, G. Chulkova, A. Korneev, K. Smirov, G. N. Gol'tsman, and A. Semenov, "Detection efficiency of large-active-area NbN single-photon superconducting detectors in the ultraviolet to near-infrared," *Appl. Phys. Lett.*, vol. 80, pp. 4687–4689, Jun. 2002.

[42] A. Korneev, P. Kouminov, V. Matvienko, G. Chulkova, K. Smirnov, B. Voronov, G. N. Golt'sman, M. Currie, W. Lo, K. Wilsher, J. Zhang, W. Słysz, A. Pearlman, A. Verevkin, and R. Sobolewski, "Sensitivity and gigahertz counting performance of NbN superconducting single-photon detectors," *Appl. Phys. Lett.*, vol. 84, pp. 5338–5430, Jun. 2004.

[43] A. Verevkin, A. Pearlman, W. Słysz, J. Zhang, M. Currie, A. Korneev, G. Chulkova, O. Okunev, P. Kouminov, K. Smirnov, B. Voronov, G. N. Gol'tsman, and R. Sobolewski, "Ultrafast single-photon detectors for near-infrared-wavelength quantum communications," *J. Mod. Opt.*, vol. 51, pp. 1447–1458, Jun. 2004.

[44] R. H. Hadfield, M. J. Stevens, S. G. Gruber, A. J. Miller, R. E. Schwall, R. P. Mirin, and S. W. Nam, "Single photon source characterization with a superconducting single photon detector," *Opt. Express*, vol. 13, pp. 10846–10853, Dec. 2005.

[45] M. J. Stevens, R. H. Hadfield, R. E. Schwall, S. W. Nam, R. P. Mirin, and J. A. Gupta, "Fast lifetime measurements of infrared emitters using a low-jitter superconducting single photon detector," *Appl. Phys. Lett.*, vol. 89, pp. 031109-1–031109-3, Jul. 2006.

[46] R. Hanbury-Brown and R. Q. Twiss, "Correlation between photons in two coherent beams of light," *Nature*, vol. 117, pp. 27–29, Jan. 1956.

[47] J. G. Rarity, S. C. Kitson, and P. R. Tapster, *Confined Photon Systems: Fundamentals and Applications*, vol. 531, H. Benisty, J. M. Gérard, R. Houdré, J. Rarity, and C. Weisbuch, Eds. Berlin, Germany: Springer-Verlag, p. 352.

[48] R. Loudon, *The Quantum Theory of Light*, 3rd ed. New York: Oxford Univ. Press, 2000.

[49] C. Kurtsiefer, P. Zarda, S. Mayer, and H. Weinfurter, "The breakdown flash of silicon avalanche photodiodes–back door for eavesdropper attacks?," *J. Mod. Opt.*, vol. 48, pp. 2039–2047, Nov. 2001.

[50] G. Ulu, A. V. Sergienko, and M. S. Ünlu, "Influence of hot-carrier luminescence from avalanche photodiodes on time-correlated photon detection," *Opt. Lett.*, vol. 25, pp. 758–760, May 2000.

[51] S. Rodt, R. Heitz, R. L. Sellin, A. Schliwa, K. Pötschke, and D. Bimberg, "Biexcitons in self-organized InAs/GaAs quantum dots: An optical probe for structural properties," *Physica E*, vol. 21, pp. 1065–1069, 2004.
[52] V. D. Kulakovskii, G. Bacher, R. Weigand, T. Kümmel, A. Forchel, E. Borovitskaya, K. Leonardi, and D. Hommel, "Fine structure of biexciton emission in symmetric and asymmetric CdSe/ZnSe single quantum dots," *Phys. Rev. Lett.*, vol. 82, pp. 1780–1783, Feb. 2003.
[53] A. Imamoğlu and Y. Yamamoto, "Turnstile device for heralded single photons: Coulomb blockade of electron and hole tunneling in quantum confined p-i-n heterojunctions," *Phys. Rev. Lett.*, vol. 72, pp. 210–213, Jan. 1994.
[54] A. S. Shkolnik, L. Ya Karachinsky, N. Yu. Gordeev, G. G. Zegrya, V. P. Evtikhiev, S. Pellegrini, and G. S. Buller, "Observation of the biexponential ground-state decay time behavior in InAs self-assembled quantum dots grown on misoriented substrates," *Appl. Phys. Lett.*, vol. 86, no. 21, pp. 211112-1–211112-3, May 2005.
[55] N. Baer, C. Gies, J. Wiersig, and F. Jahnke, "Luminescence of a semiconductor quantum dot system," *Eur. Phys. J. B*, vol. 50, pp. 411–418, Dec. 2005.
[56] G. N. Gol'tsman, A. Korneev, I. Rubtsova, I. Milostnaya, G. Chulkova, O. Minaeva, K. Smirnov, B. Voronov, W. Słysz, A. Pearlman, A. Verevkin, and R. Sobolewski, "Ultrafast superconducting single-photon detectors for near-infrared-wavelength quantum communications," *Physica Status Solidi C*, vol. 2, pp. 1480–1488, Mar. 2005.
[57] R. H. Hadfield, A. J. Miller, S. W. Nam, R. L. Kautz, and R. E. Schwall, "Low-frequency phase locking in high-inductance superconducting nanowires," *Appl. Phys. Lett.*, vol. 87, pp. 203505-1–203505-3, Nov. 2005.
[58] A. J. Kerman, E. A. Dauler, W. E. Keicher, J. K. W. Yang, K. K. Berggren, G. Gol'tsman, and B. Voronov, "Kinetic-inductance-limited reset time of superconducting nanowire photon counters," *Appl. Phys. Lett.*, vol. 88, pp. 111116-1–111116-3, Mar. 2006.
[59] A. D. Semenov, G. N. Gol'tsman, and A. A. Korneev, "Quantum detection by current carrying superconducting film," *Physica C*, vol. 351, pp. 349–356, Apr. 2001.
[60] R. Radebaugh, "Refrigeration for superconductors," *Proc. IEEE*, vol. 92, no. 10, pp. 1719–1734, Oct. 2004.
[61] R. Krahl, A. Bülter, and F. Koberling. (2005) Performance of the micro photon devices PDM 50CT SPAD detector with PicoQuant TCSPC systems. Pico Quant GmbH. Berlin, Germany. [Online]. Available: http://www.picoquant.com/_scientific.htm
[62] A. Spinelli, M. A. Ghioni, S. D. Cova, and L. M. Davis, "Avalanche detector with ultraclean response for time-resolved photon counting," *IEEE J. Quantum Electron.*, vol. 34, no. 5, pp. 817–821, May 1998.
[63] R. Heitz, M. Veit, N. N. Ledentsov, A. Hoffmann, D. Bimberg, V. M. Ustinov, P. S. Kop'ev, and Z. I. Alferov, "Energy relaxation by multiphonon processes in InAs/GaAs quantum dots," *Phys. Rev. B, Condens. Matter*, vol. 56, pp. 10435–10444, Oct. 1997.
[64] D. Dalacu, D. Poitras, J. Lefbevre, P. J. Poole, G. C. Aers, and R. L. Williams, "InAs/InP quantum dot pillar microcavities using SiO_2/Ta_2O_5 Bragg reflectors with emission around 1.5 μm," *Appl. Phys. Lett.*, vol. 84, pp. 3235–3237, Apr. 2004.
[65] B. Alloing, C. Zinoni, V. Zwiller, L. H. Li, C. Monat, M. Gobet, T. Buchs, A. Fiore, E. Pelucchi, and E. Kapon, "Growth and characterization of single quantum dots emitting at 1300 nm," *Appl. Phys. Lett.*, vol. 86, pp. 101908-1–101908-3, Mar. 2005.
[66] M. B. Ward, O. Z. Karimov, D. C. Unitt, Z. L. Yuan, P. See, D. G. Gevauz, A. J. Shields, P. Atkinson, and D. A. Ritchie, "On demand single photon source for 1.3 μm telecom fiber," *Appl. Phys. Lett.*, vol. 86, pp. 201111-1–201111-3, May 2005.

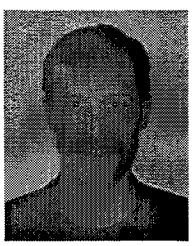

Martin J. Stevens received the B.S. degree in physics from the University of Minnesota, Twin Cities, in 1996, and the Ph. D. degree in electrical and computer engineering from the University of Iowa, Iowa City, in 2004. His study focused on the fundamental interactions of carriers in semiconductors using polarization-resolved spectral interferometry. He also refined techniques for coherently controlling electron spin in semiconductors, including the all-optical injection and control of ballistic spin currents.

He is currently a Postdoctoral Fellow at the National Institute of Standards and Technology (NIST), Boulder, CO. At NIST, he has worked on advanced spectroscopy and other measurement techniques for characterizing quantum dot single photon sources. His current research interests include implementing quantum dots in fundamental quantum optics experiments.

Dr. Stevens is a member of the Optical Society of America and the American Physical Society.

Robert H. Hadfield received the B.A. and M.Sci. degrees in natural sciences (physics) in 1998 and the Ph.D. degree in materials science in 2003 from the University of Cambridge, Cambridge, U.K. His study centered on nanoscale Josephson junctions fabricated by focused ion beam microscope.

In 2003, he joined the National Institute of Standards and Technology (NIST), Boulder, CO, as a Postdoctoral Guest Researcher. His current research interests include the fabrication, testing, and implementation of ultrafast infrared superconducting single-photon detectors for applications in quantum information. In January 2007, he will join the Department of Physics, Heriot-Watt University, Edinburgh, U.K., as a Royal Society University Research Fellow.

Dr. Hadfield is a member of the America Physical Society, the Optical Society of America, and the U.K. Institute of Physics.

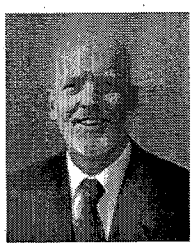

Robert E. Schwall (M'91–SM'98) received the B.S. degreee in physics from St. Mary's University, San Antonio, TX, in 1968, and the M.S. and Ph.D. degrees in applied physics from Stanford University, Stanford, CA, in 1969 and 1972, respectively.

From 1984 to 1993, he was with IBM, where he was the Manager of the Optical Systems Group, Thomas J. Watson Research Laboratory. He also led a project addressing the packaging and cooling of CMOS circuits operating at cryogenic temperatures. From 1993 to 2003, he held a number of positions at American Superconductor Corporation, Westborough MA, including that of Vice President of Engineering, leading the development of the high-temperature superconductors BSCCO and thin film YBCO. He is currently the Project Leader of the Quantum Information and Measurements Project at the National Institute of Standards and Technology (NIST), Boulder, CO. His current research includes quantum computing, quantum circuits incorporating single electron devices, and cryogen-free systems incorporating superconducting sensors. He has authored over 60 patents and refereed publications.

Dr. Schwall is a Fellow of the American Physical Society.

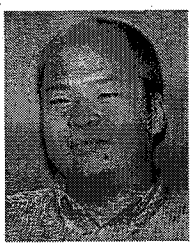

Sae Woo Nam (M'05) received the B.S. degree in electrical engineering and physics from Massachusetts Institute of Technology, Cambridge, in 1991, and the M.S. and Ph.D degrees in physics from Stanford University, Stanford, CA, in 1999.

He was an NRC Postdoctoral Fellow at the National Institute of Standards and Technology (NIST), Boulder, CO. His research focused on advanced applications of superconducting Transition-Edge Sensor (TES) based detectors. He was recently hired full time at NIST to continue this and other advanced metrology work. His current research interests include using superconducting detectors (TES and SSPD) for direct detection of photons at telecommunications and optical wavelengths for astronomical observations and quantum information applications.

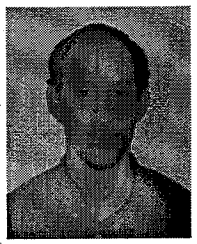

Richard P. Mirin (S'87–M'90–SM'05) received the B.S. degree in electrical engineering from the University of California, Berkeley, in 1990, and the M.S. and Ph.D. degrees in electrical engineering from the University of California, Santa Barbara, in 1992 and 1996, respectively.

He joined the Optoelectronics Division, National Institute of Standards and Technology (NIST), Boulder, CO, where he is currently the Project Leader for the Nanostructure Fabrication and Metrology Project. His current research interests include precision spectroscopy of semiconductor quantum dots and the applications of quantum dots for single photon sources and detectors. He has authored more than 50 journal papers and 80 conference presentations and proceedings papers.

Dr. Mirin is a member of the Optical Society of America.